Acoustic streaming in simplified liquid rocket engines with transverse mode oscillations

Sean R. Fischbach, Gary A. Flandro, and Joseph Majdalani[a)]
Mechanical, Aerospace and Biomedical Engineering Department, University of Tennessee (UTSI), Tullahoma, Tennessee 37388-9700, USA

(Received 25 June 2009; accepted 2 March 2010; published online 7 June 2010)

This study considers a simplified model of a liquid rocket engine in which uniform injection is imposed at the faceplate. The corresponding cylindrical chamber has a small length-to-diameter ratio with respect to solid and hybrid rockets. Given their low chamber aspect ratios, liquid thrust engines are known to experience severe tangential and radial oscillation modes more often than longitudinal ones. In order to model this behavior, tangential and radial waves are superimposed onto a basic mean-flow model that consists of a steady, uniform axial velocity throughout the chamber. Using perturbation tools, both potential and viscous flow equations are then linearized in the pressure wave amplitude and solved to the second order. The effects of the headwall Mach number are leveraged as well. While the potential flow analysis does not predict any acoustic streaming effects, the viscous solution carried out to the second order gives rise to steady secondary flow patterns near the headwall. These axisymmetric, steady contributions to the tangential and radial traveling waves are induced by the convective flow motion through interactions with inertial and viscous forces. We find that suppressing either the convective terms or viscosity at the headwall leads to spurious solutions that are free from streaming. In our problem, streaming is initiated at the headwall, within the boundary layer, and then extends throughout the chamber. We find that nonlinear streaming effects of tangential and radial waves act to alter the outer solution inside a cylinder with headwall injection. As a result of streaming, the radial wave velocities are intensified in one-half of the domain and reduced in the opposite half at any instant of time. Similarly, the tangential waves are either enhanced or weakened in two opposing sectors that are at 90° angle to the radial velocity counterparts. The second-order viscous solution that we obtain clearly displays both an oscillating and a steady flow component. The steady part can be an important contributor to wave steepening, a mechanism that is often observed during the onset of acoustic instability.
 [doi:10.1063/1.3407663]

I. INTRODUCTION

Combustion instability in liquid rocket engines is characterized by large amplitude pressure fluctuations, elevated mean pressures, and frequencies that closely match linear chamber acoustics.[1,2] Owing to this fact, analytical methodologies put forward to describe flow oscillations lean heavily on the assumption of small acoustic disturbances.[3–17] Contrary to this assumption, however, a vast body of experimental evidence conveys a dissimilar picture, specifically, one involving large amplitude oscillations with steep gradients in flow variables. For example, in the extensive experimental studies of Clayton, Sotter, and co-workers,[18–21] a heavily instrumented, laboratory scale, 20 000 lbf thrust engine was used to investigate high amplitude tangential oscillations. Their measurements exhibited sustained, steep-fronted pressure fluctuations with peak-to-peak amplitudes that were an order of magnitude larger than the chamber's operating pressure. The pressure transducers available at the time could not record data rapidly enough to determine if a true discontinuity was present, but the acquired wave forms displayed large amplitude spikes followed by long and shallow pressure segments.

Theoretical work attributed to Maslen and Moore[22] suggested that tangential waves could not steepen as in the case of plane waves. In their 1956 paper, these investigators studied the effects of secondary flows on tangential wave patterns. A circular cylinder with a zero mean flow was utilized to detail the interaction between tangential waves and the chamber's sidewall. Specifically, the secondary flow induced by viscous forces at the sidewall was described. Their analysis yielded a streaming profile that acted in the direction opposite to the wave spinning motion. As a result, it was speculated that steep fronted, shocklike waves could not be produced due to sidewall scattering and viscous dissipation. Later, a study by Flandro[23] that incorporated a mean flow along with mass transpiration from the sidewall predicted a streaming flow in the same direction as the first-order wave. This result was found to be dependent on the magnitude of the injection Mach number. Given the dissimilar views in the role of acoustic streaming on the production of transverse traveling waves, its origination, manifestation, and influence on wave steepening will be the chief focus of this study.

With extensive work already in place for the treatment of radial boundary layers forming over an injecting

a)Author to whom correspondence should be addressed. Telephone: (931) 393-7280. Fax: (931) 393-7530. Electronic mail: maji@utsi.edu.

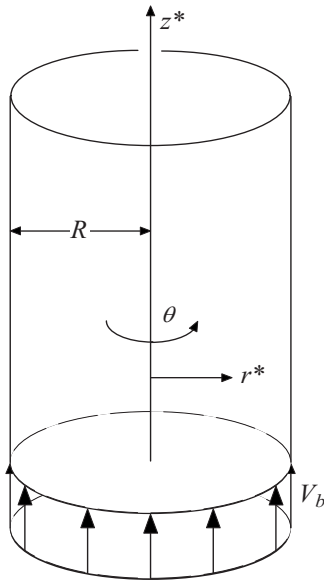

FIG. 1. Chamber geometry and coordinate system.

sidewall,[24–28] the present article also seeks to investigate the structure of the unsteady axial boundary layers forming over an injecting headwall in the presence of transverse waves. The motivation to tackle the axial boundary layer analog is inspired by experimental observations suggesting that the highest pressure amplitudes and therefore most severe waves often occur near the injector face.[18–21]

The mechanisms that cause a plane wave to steepen are well understood. At the pressure peak the local speed of sound is elevated, thus increasing the local wave propagation rate. At the outset, the crest of the wave overtakes the depressed pressure portion. The curled-up wave continues to steepen until the solution becomes multivalued when nonlinear forces act to reverse this trend. The present study will demonstrate how secondary streaming flows induced at a liquid engine's injector face can stimulate a similar steepening process for tangentially traveling waves. In order to model this behavior, tangential and radial waves will be superimposed onto a simple mean-flow model. Considerable effort will then be given to satisfy the no-slip condition at the engine's injector face. The representative geometry, displayed in Fig. 1, will correspond to that of a semi-infinite cylinder of radius R with a suitable coordinate system anchored at the chamber's headwall. The z-coordinate will be located along the chamber's centerline.

II. FORMULATION

For simplicity, we begin the analysis by normalizing all standard variables bearing an asterisk according to

$$\begin{cases} p = p^*/P_0 & \mathbf{u} = \mathbf{u}^*/a_0 & r = r^*/R & T = T^*/T_0 \\ \rho = \rho^*/\rho_0 & t = t^*/(R/a_0) & z = z^*/R & \varpi = \varpi^*/(a_0/R) \end{cases}, \tag{1}$$

where ϖ and a_0 denote the circular frequency and speed of sound, respectively; as usual, the zero subscript is used to denote a mean flow property. Using $\boldsymbol{\omega} = \nabla \times \boldsymbol{u}$ to denote the vorticity, the dimensionless equations written for a viscous compressible fluid consist of

$$\frac{\partial \rho}{\partial t} + \nabla \cdot (\rho \mathbf{u}) = 0 \quad \text{(continuity)}, \tag{2}$$

$$\rho\left(\frac{\partial \mathbf{u}}{\partial t} + \frac{1}{2}\nabla \mathbf{u}^2 - \mathbf{u} \times \boldsymbol{\omega}\right) = -\frac{1}{\gamma}\nabla p - \delta^2 \nabla \times (\nabla \times \mathbf{u}) + \delta_d^2 \nabla (\nabla \cdot \mathbf{u}) + \mathbf{F} \quad \text{(momentum)}, \tag{3}$$

$$p = \rho T \quad \text{(state)}, \tag{4}$$

$$p = \rho^\gamma \quad \text{(isentropic relation)}. \tag{5}$$

Here $\mathbf{F}$ is the body force whereas the viscous and dilatational parameters that appear in Eq. (3) are defined as

$$\delta = \sqrt{\nu/(a_0 R)}; \quad \delta_d = \delta\sqrt{\mu'/\mu + \tfrac{4}{3}}. \tag{6}$$

The symbols $\nu = \mu/\rho$, μ', and γ represent the kinematic viscosity, the second coefficient of viscosity, and the ratio of specific heats, respectively. The energy and species diffusion equations are not listed due to the analysis being based on a nonreactive, single-phase, homogeneous, calorically perfect gas assumption.

A. Unsteady flow equations

Decomposing the flow variables into steady and unsteady parts can be achieved by setting

$$\mathbf{u} = \overline{\mathbf{U}} + \mathbf{u}'; \quad \boldsymbol{\omega} = \overline{\boldsymbol{\Omega}} + \boldsymbol{\omega}'; \quad p = \bar{P} + p'; \quad \rho = \bar{\rho} + \rho'; \quad T = \bar{T} + T', \tag{7}$$

where overbars denote mean flow properties and primes represent unsteady variables. Having normalized the velocity by the speed of sound, the mean flow component may be related to the headwall injection Mach number $M_b = V_b/a_0$ using $\overline{\mathbf{U}} = M_b \mathbf{U}$. Vorticity is similarly expressed as $\overline{\boldsymbol{\Omega}} = M_b \boldsymbol{\Omega}$. Direct substitution of Eq. (7) into the governing equations enables us to isolate two sets of steady and unsteady equations. Subsequently, a perturbation expansion may be implemented to linearize the unsteady equations. This is accomplished by expanding each fluctuation a' in terms of a sequence in the pressure wave parameter,

$$a' = \varepsilon a^{(1)} + \varepsilon^2 a^{(2)} + \varepsilon^3 a^{(3)} + \cdots. \tag{8}$$

Here a represents a generic flow variable, and ε is the wave parameter, the ratio of the unsteady pressure amplitude and the mean pressure. Retaining terms to the second order in ε enables us to capture the acoustic streaming effect. As elegantly described by Schlichting[29] (p. 431), the secondary, streaming flow "has its origin in the convective terms and is due to the interaction between inertia and viscosity."

TABLE I. Boundary conditions for both potential and viscous flow analyses.

	Boundary		
	$r=R$	$z=0$	$z=L$
Potential flow	$\mathbf{n}\cdot\nabla p'=0\rightarrow u_r'=0$	$\mathbf{n}\cdot\nabla p'=0\rightarrow u_z'=0$	$\mathbf{n}\cdot\nabla p'=0\rightarrow u_z'=0$
Viscous flow	No condition imposed	No slip: $u_r'=u_\theta'=u_z'=0$	Potential flow (matching)

Furthermore, "simplifications in which the convective terms have been omitted lead to solutions which are free from streaming and may, therefore, give a misleading representation of the flow. Streaming does, in general, appear only when the solution is carried out to at least the second-order approximation." Bearing this requirement in mind, we perform some algebra and collect the first and second-order sets of equations, specifically,

$$\begin{cases} \dfrac{\partial \rho^{(1)}}{\partial t} = -\nabla\cdot\mathbf{u}^{(1)} - M_b\nabla\cdot[\rho^{(1)}\mathbf{U}] \\ \dfrac{\partial \mathbf{u}^{(1)}}{\partial t} + M_b\rho^{(1)}\dfrac{\partial \mathbf{U}}{\partial t} - M_b^2\rho^{(1)}\mathbf{U}\times\boldsymbol{\Omega} = -\dfrac{\nabla p^{(1)}}{\gamma} - M_b[\mathbf{u}^{(1)}\cdot\nabla\mathbf{U} + \mathbf{U}\cdot\nabla\mathbf{u}^{(1)}] + \mathbf{F}^{(1)} + M_b\mathbf{u}^{(1)}\times\boldsymbol{\Omega} + M_b\mathbf{U}\times\boldsymbol{\omega}^{(1)} \\ \qquad\qquad - \delta^2\nabla\times\boldsymbol{\omega}^{(1)} + \delta_d^2\nabla[\nabla\cdot\mathbf{u}^{(1)}] \\ p^{(1)} = T^{(1)} + \rho^{(1)} \end{cases}, \tag{9}$$

and

$$\begin{cases} \dfrac{\partial \rho^{(2)}}{\partial t} = -\nabla\cdot\mathbf{u}^{(2)} - \nabla\cdot[\rho^{(1)}\mathbf{u}^{(1)}] - M_b\nabla\cdot[\rho^{(2)}\mathbf{U}] \\ \dfrac{\partial \mathbf{u}^{(2)}}{\partial t} + M_b\rho^{(2)}\dfrac{\partial \mathbf{U}}{\partial t} - M_b^2\rho^{(2)}\mathbf{U}\times\boldsymbol{\Omega} = -\dfrac{\nabla p^{(2)}}{\gamma} - M_b\{\mathbf{u}^{(2)}\cdot\nabla\mathbf{U} + \mathbf{U}\cdot\nabla\mathbf{u}^{(2)} + \rho^{(1)}[\mathbf{u}^{(1)}\cdot\nabla\mathbf{U} + \mathbf{U}\cdot\nabla\mathbf{u}^{(1)}]\} \\ \qquad\qquad - \dfrac{1}{2}\rho^{(2)}M_b^2\mathbf{U}\cdot\nabla\mathbf{U} + \rho^{(1)}M_b\mathbf{U}\times\boldsymbol{\omega}^{(1)} + M_b\rho^{(1)}\mathbf{u}^{(1)}\times\boldsymbol{\Omega} + M_b\mathbf{U}\times\boldsymbol{\omega}^{(2)} \\ \qquad\qquad + \mathbf{u}^{(1)}\times\boldsymbol{\omega}^{(1)} - \rho^{(1)}\dfrac{\partial \mathbf{u}^{(1)}}{\partial t} - \mathbf{u}^{(1)}\cdot\nabla\mathbf{u}^{(1)} + \mathbf{F}^{(2)} - \delta^2\nabla\times\boldsymbol{\omega}^{(2)} + \delta_d^2\nabla[\nabla\cdot\mathbf{u}^{(2)}] \\ p^{(2)} = T^{(2)} + T^{(1)}\rho^{(1)} + \rho^{(2)} \end{cases}. \tag{10}$$

To set the stage, our plan is to apply a procedure that will require the construction of both a potential (outer) solution and a corresponding viscous (inner) solution. The boundary conditions that will be employed in each part of the analysis are cataloged in Table I. Accordingly, the potential motion will be subject to the rigid wall boundary condition through which the flow velocity is required to vanish at the chamber walls. The viscous flow solution, on the other hand, will make use of the no-slip condition at the injector face, at $z=0$, where acoustic streaming is triggered. In applying the concepts of matched asymptotic theory, the potential flow solution will be used as the outer, farfield boundary for the viscous expansion. Finally, the thin boundary layer forming along the lateral wall, at $r=R$, will be ignored, consistently with the assumption of a proportionately large circular faceplate relative to a thin viscous region.

B. Headwall injection flow field

It may be instructive to note that Eqs. (9) and (10) represent the interaction equations that prescribe the unsteady wave motion in an idealized liquid rocket thrust engine. Both expressions of mass conservation and momentum balance are strongly influenced by the headwall injection Mach number M_b and the mean flow field velocity function $\mathbf{U}$. In the context of a liquid rocket chamber, we recognize that the injection process at the headwall can be superbly complex. However, we also realize that despite the inherent complexity of the injection patterns, a streamtube motion is quickly established. Bearing these factors in mind, we adopt a simple representation of the mean flow field that consists of a uniform stream with constant velocity. This basic approximation will be necessary to simplify the problem and, in the process, help elucidate the underpinning physical mechanisms with

minimal algebraic encumbrance. Further complexity in the mean flow definition can be pursued at a later time. It should be kept in mind, however, that the uniform flow assumption is accompanied by certain limitations; these will be brought to light later in the analysis. With the near injector faceplate as the principal region of interest, we assume steady injection. We then introduce the nondimensional mean flow $\overline{\mathbf{U}}=M_b\mathbf{U}$ where

$$\mathbf{U}=\mathbf{e}_z. \tag{11}$$

This basic representation is illustrated in Fig. 1.

III. POTENTIAL FLOW SOLUTION

Away from the headwall region, viscous effects are confined to a thin boundary layer along the lateral, noninjecting sidewall. At the outset, a potential inviscid field may be assumed in the downstream region that is sufficiently removed from the injectors. Such a potential flow representation plays the role of an outer solution with respect to the flow adjacent to the headwall. By discounting viscosity, one is left with a set of wavelike equations that are described next.

A. First-order potential solution

A combination of the first-order momentum and continuity equations delivers an expression for the unsteady wave motion to $\mathcal{O}(\varepsilon)$. Then, given the isentropic flow assumption, linearization of the pressure and density relation given by Eq. (5) yields

$$\gamma\rho^{(1)}=p^{(1)}. \tag{12}$$

As usual, constructing the wave equation requires taking the time derivative of the continuity equation and subtracting from it the divergence of the momentum equation. One readily obtains

$$\nabla^2 p^{(1)}-p_{tt}^{(1)}=-\frac{\partial}{\partial t}\{M_b\nabla\cdot[p^{(1)}\mathbf{U}]\}+\gamma M_b\nabla^2[\mathbf{U}\cdot\mathbf{u}^{(1)}]. \tag{13}$$

Given that the right-hand side in the above is of $\mathcal{O}(M_b)$, the first-order pressure can be represented by a dual perturbation expansion in M_b. Then to seek general solutions for $p^{(1)}$ and $\mathbf{u}^{(1)}$, we first derive general expressions for the expanded subcomponents, $p^{(1,0)}$ and $\mathbf{u}^{(1,0)}$. Thus using a' to denote a generic fluctuating variable, each level in the pressure wave parameter may be extended successively as

$$\begin{cases} a'=\varepsilon[a^{(1,0)}+M_b a^{(1,1)}+M_b^2 a^{(1,2)}+\cdots]+\varepsilon^2[a^{(2,0)}+M_b a^{(2,1)}+M_b^2 a^{(2,2)}+\cdots]+\cdots \\ p'=\varepsilon[p^{(1,0)}+M_b p^{(1,1)}+M_b^2 p^{(1,2)}+\cdots]+\varepsilon^2[p^{(2,0)}+M_b p^{(2,1)}+M_b^2 p^{(2,2)}+\cdots]+\cdots \\ \mathbf{u}'=\varepsilon[\mathbf{u}^{(1,0)}+M_b\mathbf{u}^{(1,1)}+M_b^2\mathbf{u}^{(1,2)}+\cdots]+\varepsilon^2[\mathbf{u}^{(2,0)}+M_b\mathbf{u}^{(2,1)}+M_b^2\mathbf{u}^{(2,2)}+\cdots]+\cdots \end{cases} \tag{14}$$

or

$$\begin{cases} p^{(1)}=p^{(1,0)}+M_b p^{(1,1)}+M_b^2 p^{(1,2)}+\cdots \\ p^{(2)}=p^{(2,0)}+M_b p^{(2,1)}+M_b^2 p^{(2,2)}+\cdots \\ \mathbf{u}^{(1)}=\mathbf{u}^{(1,0)}+M_b\mathbf{u}^{(1,1)}+M_b^2\mathbf{u}^{(1,2)}+\cdots \\ \mathbf{u}^{(2)}=\mathbf{u}^{(2,0)}+M_b\mathbf{u}^{(2,1)}+M_b^2\mathbf{u}^{(2,2)}+\cdots \end{cases}. \tag{15}$$

Subsequent expansions of the first-order wave equation yield

$$\begin{cases} \nabla^2 p^{(1,0)}-p_{tt}^{(1,0)}=0 \\ \mathbf{n}\cdot\nabla p^{(1,0)}|_{z=0}=0;\quad \mathbf{n}\cdot\nabla p^{(1,0)}|_{r=1}=0 \end{cases}, \tag{16}$$

$$\begin{cases} \nabla^2 p^{(1,1)}-p_{tt}^{(1,1)}=-\mathbf{U}\cdot\nabla p_t^{(1,0)}+\gamma\nabla^2[\mathbf{U}\cdot\mathbf{u}^{(1,0)}] \\ \mathbf{n}\cdot\nabla p^{(1,1)}|_{z=0}=0;\quad \mathbf{n}\cdot\nabla p^{(1,1)}|_{r=1}=0 \end{cases}, \tag{17}$$

and

$$\begin{cases} \nabla^2 p^{(1,2)}-p_{tt}^{(1,2)}=-\mathbf{U}\cdot\nabla p_t^{(1,1)}+\gamma\nabla^2[\mathbf{U}\cdot\mathbf{u}^{(1,1)}] \\ \mathbf{n}\cdot\nabla p^{(1,2)}|_{z=0}=0;\quad \mathbf{n}\cdot\nabla p^{(1,2)}|_{r=1}=0 \end{cases}. \tag{18}$$

Note that the appropriate boundary condition forces the normal projection of the pressure gradient to vanish at all chamber surfaces. To solve Eq. (16), separation of variables may be used to derive the first-order pressure in the form of $p^{(1,0)}=F(r)G(\theta)H(z)\Gamma(t)$. At the outset, the wave equation collapses into

$$\frac{d^2F}{dr^2}\frac{1}{F}+\frac{1}{r}\frac{dF}{dr}\frac{1}{F}+\frac{1}{r^2}\frac{d^2G}{d\theta^2}\frac{1}{G}-\frac{d^2\Gamma}{dt^2}\frac{1}{\Gamma}=-\frac{d^2H}{dz^2}\frac{1}{H}=k_l^2. \tag{19}$$

Equation (19) may be rearranged into

$$\begin{cases} \dfrac{d^2F}{dr^2}\dfrac{1}{F}+\dfrac{1}{r}\dfrac{dF}{dr}\dfrac{1}{F}+\dfrac{1}{r^2}\dfrac{d^2G}{d\theta^2}\dfrac{1}{G}-\dfrac{d^2\Gamma}{dt^2}\dfrac{1}{\Gamma}-k_l^2=0 \\ \dfrac{d^2H}{dz^2}+k_l^2H=0 \end{cases}. \tag{20}$$

On this basis, a longitudinal wave solution of the form $H(z)=\cos(k_l z)$ may be realized. In the present work, the longitudinal wave number k_l is deliberately set to zero in order to isolate the tangential and radial wave contributions. One is left with the radial, azimuthal, and temporal ODEs,

$$r^2\frac{d^2F}{dr^2}\frac{1}{F}+r\frac{dF}{dr}\frac{1}{F}-r^2\frac{d^2\Gamma}{dt^2}\frac{1}{\Gamma}=-\frac{d^2G}{d\theta^2}\frac{1}{G}=m^2. \tag{21}$$

So on the one hand, knowing that the θ-dependence cannot be multivalued, $G(\theta)$ becomes

$$G=A_\theta e^{im\theta}. \tag{22}$$

On the other hand, the radial and temporal dependence may be separated from

$$\frac{d^2F}{dr^2}\frac{1}{F}+\frac{1}{r}\frac{dF}{dr}\frac{1}{F}-\frac{m^2}{r^2}=\frac{d^2\Gamma}{dt^2}\frac{1}{\Gamma}=-K^2, \tag{23}$$

or

$$\begin{cases}\dfrac{d^2F}{dr^2}\dfrac{1}{F}+\dfrac{1}{r}\dfrac{dF}{dr}\dfrac{1}{F}+\left(K^2-\dfrac{m^2}{r^2}\right)=0\\ \dfrac{d^2\Gamma}{dt^2}+K^2\Gamma=0\end{cases}. \tag{24}$$

The classical form of the solution to Eq. (24) gives

$$F=A_rJ_m(k_{mn}r)+B_rY_m(k_{mn}r), \tag{25}$$

where $k_{mn}\equiv K$ and (J_m,Y_m) represent the mth order Bessel functions of the first and second kind, respectively. In the time domain the solution to Eq. (24) can be represented by complex variables as

$$\Gamma=e^{-ik_{mn}t}, \tag{26}$$

with $k_{mn}=\varpi_0R/a_0$. For the assumed sinusoidal variation in time, initial conditions are immaterial to the character of the solution. Without loss of generality, the product of tangential, radial, and temporal contributions may be expressed as

$$p_c^{(1,0)}=[AJ_m(k_{mn}r)e^{im\theta}+BY_m(k_{mn}r)e^{im\theta}]e^{-ik_{mn}t}. \tag{27}$$

Where the subscript c denotes a complex variable. Equation (27) admits a finite pressure at the centerline (i.e., $B=0$) and a vanishing pressure gradient at the impermeable wall, $J'_m(k_{mn})=0$. Using unit normalization Eq. (27) becomes

$$p_c^{(1,0)}=J_m(k_{mn}r)e^{i(m\theta-k_{mn}t)}. \tag{28}$$

Subsequently, care is exerted in extracting the real component of a given variable before substitution back into the governing equations that are constructed assuming real quantities. For example, $p^{(1,0)}$, the first order in ε and zeroth order in M_b approximation for the pressure becomes

$$p^{(1,0)}=\cos(m\theta-k_{mn}t)J_m(k_{mn}r);\qquad m=0,1,2,\ldots;\quad n=0,1,2,\ldots, \tag{29}$$

where k_{mn} is determined by the roots of the first derivative of the Bessel function of order m, $J'_m(k_{mn})=0$. One finds

$$k_{01}\simeq 3.831\,705\,97,\quad k_{10}\simeq 1.841\,183\,78,$$

$$k_{11}\simeq 5.331\,442\,77,\quad k_{02}\simeq 7.0155\,866\,7, \tag{30}$$

$$k_{20}\simeq 3.054\,236\,93,\quad \text{etc.}$$

Being chiefly concerned with the effect of tangential wave motion at the headwall, the first spinning mode of interest is k_{10}. Note that Eq. (29) captures both tangential and radial oscillation modes. Using Eqs. (9) and (14) produces a set of equations representing the first-order potential velocity

$$\begin{cases}\dfrac{\partial\mathbf{u}^{(1,0)}}{\partial t}=-\dfrac{\nabla p^{(1,0)}}{\gamma}\\ \mathbf{n}\cdot\mathbf{u}^{(1,0)}|_{z=0}=0;\quad \mathbf{n}\cdot\mathbf{u}^{(1,0)}|_{r=1}=0\end{cases}, \tag{31}$$

$$\begin{cases}\dfrac{\partial\mathbf{u}^{(1,1)}}{\partial t}=-\dfrac{\nabla p^{(1,1)}}{\gamma}-\mathbf{u}^{(1,0)}\cdot\nabla\mathbf{U}-\mathbf{U}\cdot\nabla\mathbf{u}^{(1,0)}\\ \mathbf{n}\cdot\mathbf{u}^{(1,1)}|_{z=0}=0;\quad \mathbf{n}\cdot\mathbf{u}^{(1,1)}|_{r=1}=0\end{cases}, \tag{32}$$

and

$$\begin{cases}\dfrac{\partial\mathbf{u}^{(1,2)}}{\partial t}=-\dfrac{\nabla p^{(1,2)}}{\gamma}-\mathbf{u}^{(1,1)}\cdot\nabla\mathbf{U}-\mathbf{U}\cdot\nabla\mathbf{u}^{(1,1)}\\ \mathbf{n}\cdot\mathbf{u}^{(1,2)}|_{z=0}=0;\quad \mathbf{n}\cdot\mathbf{u}^{(1,2)}|_{r=1}=0\end{cases}. \tag{33}$$

The first order in ε and zeroth order in M_b inviscid velocity profile may be evaluated from Eq. (31). It gives

$$\mathbf{u}_c^{(1,0)}=-\frac{i}{\gamma K}J'_m(k_{mn}r)e^{i(m\theta-Kt)}\mathbf{e}_r+\frac{1}{\gamma K}\left(\frac{m}{r}\right)J_m(k_{mn}r)e^{i(m\theta-Kt)}\mathbf{e}_\theta, \tag{34}$$

$$\text{whence}\quad \mathbf{u}^{(1,0)}=\frac{1}{\gamma K}\sin(m\theta-k_{mn}t)J'_m(k_{mn}r)\mathbf{e}_r+\frac{1}{\gamma K}\left(\frac{m}{r}\right)\cos(m\theta-k_{mn}t)J_m(k_{mn}r)\mathbf{e}_\theta. \tag{35}$$

To avoid the pitfalls of complex notation in the evaluation of nonlinear terms, the real part of the solution featured in Eqs. (29) and (35) will be used, as the solution is taken to second order, to represent the product of two oscillatory quantities. However, complex notation will be returned to in Sec. IV A, in the treatment of the first order viscous solution. By carrying the solution to higher orders in the injection Mach number, the same recursive formulation is obtained at every order. This behavior may be attributed to the assumptions that $k_l=0$, and $U=1$, thus leading to vanishing spatial derivatives of all unsteady flow variables in the z-direction. Then by summing all terms, one deduces

$$\begin{cases} \mathbf{u}_c^{(1)} = \left(\sum_{j=0}^{\infty} M_b^j \right) \mathbf{u}_c^{(1,0)} = \dfrac{1}{1-M_b} \mathbf{u}_c^{(1,0)} \\ p_c^{(1)} = \left(\sum_{j=0}^{\infty} M_b^j \right) p_c^{(1,0)} = \dfrac{1}{1-M_b} p_c^{(1,0)} = \dfrac{J_m(k_{mn}r)}{1-M_b} e^{i(m\theta - k_{mn}t)} \end{cases}, \tag{36}$$

and so, in the real domain,

$$\begin{cases} \mathbf{u}^{(1)} = \left(\sum_{j=0}^{\infty} M_b^j \right) \mathbf{u}^{(1,0)} = \dfrac{1}{1-M_b} \mathbf{u}^{(1,0)} \\ p^{(1)} = \left(\sum_{j=0}^{\infty} M_b^j \right) p^{(1,0)} = \dfrac{1}{1-M_b} p^{(1,0)} = \dfrac{J_m(k_{mn}r)}{1-M_b} \cos(m\theta - k_{mn}t) \end{cases}. \tag{37}$$

Note that the infinite series are reducible by use of the identity

$$\sum_{j=0}^{\infty} x^j = \frac{1}{1-x}. \tag{38}$$

By summing over an infinite series in the Mach number, the solution is captured exactly in M_b, specifically with a truncation error equal to

$$\lim_{j \to \infty} M_b^j = 0. \tag{39}$$

Therefore, for the remainder of the analysis, the highly accurate solution will be represented through the use of $\mathbf{u}^{(1)}$ and $p^{(1)}$.

B. Second-order potential solution

The second-order wave equation can be retrieved at $\mathcal{O}(\varepsilon^2)$, with the outcome being

$$\begin{aligned} \nabla^2 p^{(2)} - p_{tt}^{(2)} = {} & \frac{1-\gamma}{2\gamma} \{ [p^{(1)}]^2 \}_{tt} + \nabla \cdot [p_t^{(1)} \mathbf{u}^{(1)}] \\ & - \frac{1}{2} \gamma \nabla^2 [\mathbf{u}^{(1)} \cdot \mathbf{u}^{(1)}] + M_b [\nabla \cdot p^{(2)} U]_t \\ & - \gamma M_b \nabla \cdot \nabla [\mathbf{U} \cdot \mathbf{u}^{(2)}]. \end{aligned} \tag{40}$$

Parallel expansion in the Mach number can be performed using

$$p^{(2)} = p^{(2,0)} + M_b p^{(2,1)} + M_b^2 p^{(2,2)} + \cdots. \tag{41}$$

This enables us to extract, at leading order in the Mach number and second order in the wave amplitude,

$$\begin{cases} \nabla^2 p^{(2,0)} - p_{tt}^{(2,0)} = \dfrac{1-\gamma}{2\gamma} \{ [p^{(1,0)}]^2 \}_{tt} + \nabla \cdot [p_t^{(1,0)} \mathbf{u}^{(1,0)}] - \dfrac{\gamma}{2} \nabla^2 [\mathbf{u}^{(1,0)} \cdot \mathbf{u}^{(1,0)}] \\ \mathbf{n} \cdot \nabla p^{(2,0)}|_{z=0} = 0; \quad \mathbf{n} \cdot \nabla p^{(2,0)}|_{r=1} = 0 \end{cases}. \tag{42}$$

Inserting the first-order flow field on the right-hand gives

$$\nabla^2 p^{(2,0)} - p_{tt}^{(2,0)} = F(r) + B(r) \cos[2(m\theta - k_{mn}t)], \tag{43}$$

where

$$F(r) = \frac{1}{2\gamma k_{mn}^2} \left[\begin{aligned} & \left(\frac{3m^2}{r^3} + \frac{k_{mn}^2}{r} \right) J_m(k_{mn}r) J_m'(k_{mn}r) + \left(k_{mn}^2 - \frac{m^2}{r^2} \right) J_m'^2(k_{mn}r) + \left(k_{mn}^2 - \frac{m^2}{r^2} \right) J_m(k_{mn}r) J_m''(k_{mn}r) \\ & - \frac{1}{r} J_m'(k_{mn}r) J_m''(k_{mn}r) - J_m''^2(k_{mn}r) - J_m'(k_{mn}r) J_m'''(k_{mn}r) - \frac{2m^2}{r^4} J_m^2(k_{mn}r) \end{aligned} \right], \tag{44}$$

and

$$B(r)=\frac{1}{2\gamma k_{mn}^2}\left\{\begin{array}{l} 2\left[k_{mn}^4(\gamma-1)+\dfrac{k_{mn}^2m^2}{r^2}-\dfrac{m^2(1-m^2)}{r^4}\right]J_m^2(k_{mn}r)+J_m''^2(k_{mn}r) \\ -\left(\dfrac{k_{mn}^2}{r}-\dfrac{3m^2}{r^3}\right)J_m(k_{mn}r)J_m'(k_{mn}r)-\left(k_{mn}^2+\dfrac{3m^2}{r^2}\right)J_m'^2(k_{mn}r) \\ -\left(k_{mn}^2+\dfrac{m^2}{r^2}\right)J_m(k_{mn}r)J_m''(k_{mn}r)+\dfrac{J_m'(k_{mn}r)J_m''(k_{mn}r)}{r}+J_m'(k_{mn}r)J_m'''(k_{mn}r) \end{array}\right\}. \tag{45}$$

As in the previous section, the wave equation is further expanded in terms of the injection Mach number. The approximation to the set of second-order equations displays a pattern that is of familiar type. We find

$$p^{(2)}=\sum_{j=0}^{\infty}M_b^j[(j+1)p_p^{(2,0)}+\cos(m\theta-k_{mn}t)J_m(k_{mn}r)]=\frac{p^{(2,0)}+(1-M_b)\cos(m\theta-k_{mn}t)J_m(k_{mn}r)}{(1-M_b)^2}, \tag{46}$$

where the particular solution $p_p^{(2,0)}$ is given by the juxtaposition of a steady and a time-dependent part,

$$p_p^{(2,0)}=H(r)+G(r)\cos[2(m\theta-k_{mn}t)], \tag{47}$$

with

$$H(r)=-\frac{1}{4\gamma k_{mn}^2}\left\{\left[\left(\frac{m}{r}\right)^2-k_{mn}^2\right]J_m(k_{mn}r)^2+J_m'(k_{mn}r)^2\right\}, \tag{48}$$

and

$$\left\{\begin{array}{l} G(r)=\dfrac{1}{4\gamma k_{mn}^2}\left[-\left(\dfrac{m}{r^2}+3k_{mn}^2\right)J_m(k_{mn}r)^2+J_m'(k_{mn}r)^2+4k_{mn}^4(\gamma-1)f(r)\right]; \\ f''+\dfrac{1}{r}f'-4\left(\dfrac{m^2}{r^2}-k_{mn}^2\right)f=J_m(k_{mn}r)^2. \end{array}\right. \tag{49}$$

The second-order momentum equation may be expanded along similar lines. One gets

$$\mathbf{u}^{(2)}=\sum_{j=0}^{\infty}M_b^j[(j+1)\mathbf{u}_p^{(2,0)}+\mathbf{u}^{(1,0)}]=\frac{(1-M_b)\mathbf{u}^{(1,0)}+\mathbf{u}^{(2,0)}}{(1-M_b)^2}, \tag{50}$$

where

$$\mathbf{u}_p^{(2,0)}=\left\{\begin{array}{l} -\dfrac{1}{2\gamma^2k_{mn}}[2J_m(k_{mn})J_m'(k_{mn}r)+(1-\gamma)k_{mn}^2f'(r)]\sin[2(m\theta-k_{mn}t)]\mathbf{e}_r \\ -\dfrac{1}{\gamma^2k_{mn}}\left(\dfrac{m}{r}\right)[J_m^2(k_{mn}r)+k_{mn}^2(1-\gamma)f(r)]\cos[2(m\theta-k_{mn}t)]\mathbf{e}_\theta \end{array}\right. . \tag{51}$$

Unlike the second-order pressure $p^{(2)}$, the velocity in Eq. (51) does not comprise a steady, second-order streaming component akin to the time-independent term $H(r)$ that arises in Eq. (47). In other streaming studies,[18] one may see both steady and unsteady second-order contributions to the velocity. In such models, the second order pressure gradient is either assumed or ignored. In the present study, the use of such an assumption is not required. Instead, we recall Schlichting's description[29] (p. 430), namely, that "a potential flow which is periodic with respect to time induces a steady, secondary ('streaming') motion… as a result of viscous forces." In brief, a viscous model is vitally needed to suitably capture the second-order interactions, as attempted in similar context by Maslen and Moore.[22]

IV. VISCOUS FLOW

Attention is now turned to the region directly above the headwall, specifically to the viscous boundary layer that must develop as a result of transverse shear parallel to the injector faceplate. This boundary layer is necessary to bring the transverse components of the velocity, both tangential and radial, to vanish at the surface. Friction at the headwall